Jurnal Teknologi Kedirgantaraan (JTK)
Vol. 10, No. 1, February 2025, page. 11 – 20
ISSN: 2528-2778 (Print); 2684-9704 (Online)
https://doi.org/10.35894/jtk.v10i1.187

JTK
Jurnal Teknologi Kedirgantaraan
(Journal of Aeronautical Engineering)

Aerodynamic Performance Degradation in UAV Wings Due to Bird Strike: A Finite Element and CFD Study

Budi Aji Warsiyanto*, Muhammad Hadi Widanto, Syarifah Fairuza
Department of Aeronautical Engineering, Faculty of Aerospace and Industrial Engineering, Universitas Dirgantara Marsekal Suryadarma (Unsurya), Jalan Protokol Halim Perdanakusuma, Jakarta 13610, Indonesia

Article Info

Article History:
Submitted: 30 Agustus 2024
Revised: 11 Januari 2025
Accepted: 27 Februri 2025

Keywords:
Bird strike
Unmanned aerial vehicle
Wing deformation
Aerodynamic performace
Computational fluid dynamics

ABSTRACT

Bird strikes are a threat that affects the structural integrity of aircraft, and unmanned aerial vehicles (UAVs) are no exception. Bird strikes cause changes to the shape of the wing, including the airfoil, which affects the aerodynamic performance and flight safety of the aircraft. Unlike commercial aircraft, UAV face unique risks from bird strikes due to their smaller size and lighter structure. Manufacturers must conduct various tests before a UAV is authorized for commercial use, one of which is structural strength. Numerical simulation of bird strikes is an important part of UAV component design to reduce testing costs. This study aims to analyze the structural response and aerodynamic performance of the UAV wing airfoil due to bird strike. The deformed wing geometry for computational fluid dynamics (CFD) analysis was obtained from bird strike simulations using the finite element method and the smoothed particle hydrodynamics (SPH) bird model. The deformed wing geometry is analyzed using the CFD solver to obtain the pressure distribution around the airfoil, pressure coefficient, lift, and drag. The results show that there is only positive high pressure at the leading edge of the deformed airfoil. The lift coefficient of the deformed wing is lower than that of the undeformed wing with the change of angle of attack. In contrast to the lift coefficient, the drag coefficient of the deformed wing is greater than that of the undeformed wing with a change in angle of attack, due to the disruption of the pressure distribution.

Correspondence Author:
Budi Aji Warsiyanto
Email:
budiaji@unsurya.ac.id

INTRODUCTION

Unmanned aerial vehicles (UAV) are versatile flying machines used in various applications such as remote sensing, transportation, research, and search and rescue missions. However, one critical hazard they face during flight missions is bird strikes. Such collisions can severely damage UAV components, including the wing leading edge and nose, leading to deformation or structural failure. High-speed impacts may result in bird penetration and catastrophic loss of strength, jeopardizing mission success and safety [1], [2], [3], [4], [5], [6], [7]. Thus, robust UAV designs capable of withstanding bird strikes are crucial for ensuring operational reliability and safety.

Unlike commercial aircraft, UAV face unique risks from bird strikes due to their smaller size and lighter structure. These factors make UAV more vulnerable to being perceived as threats or prey by predatory birds [8], [9]. Various studies have analyzed the structural response of aircraft and UAV to bird strikes, often focus solely on immediate structural damage and neglect the subsequent aerodynamic implications. For instance, studies on aircraft primarily investigate deformation or penetration without analyzing changes in lift or drag caused by such damage [10], [11], [12]. There remains a critical research gap in understanding how permanent deformation caused by bird strikes affects the aerodynamic performance of UAV wings, particularly in terms of altered airflow and pressure distribution around the damaged surfaces.

This study addresses the gap in current research by not only analyzing the structural response of UAV wings to bird strikes but also evaluating the impact of permanent deformation on aerodynamic performance. Using a combination of finite element analysis (FEA) and computational fluid dynamics (CFD), this research provides a comprehensive understanding of how deformed UAV wing geometries influence aerodynamic parameters such as lift, drag, and pressure distribution, which are critical for UAV stability and efficiency.

The research aims to analyze the structural response of UAV wings to bird strikes at varying collision angles using FEA software. The resulting deformed wing geometries will then be examined using CFD software to assess their aerodynamic performance compared to undeformed wings. This study seeks to establish correlations between structural deformation and aerodynamic efficiency, providing valuable insights for designing UAVs with enhanced resilience and performance against bird strikes.

METHODS

The finite element method is used to simulate the phenomenon of bird strikes [13], [14]. Smoothed particle hydrodynamics (SPH) is used to model the behavior of bird material during a collision. A numerical model was developed to analyze the dynamic response of the UAV wing structure due to bird strikes, taking into account the operational speed.

During the collision with UAV, the bird experienced element distortion and behaved like a fluid. Therefore, SPH, which is capable of addressing element distortion issues, is used for the bird model. SPH has been included in many finite element method software to address problems with high levels of element distortion [15], [16].

The shape of the bird is considered a hemispherical-ended cylinder. Barber et al. [17] investigated bird species to determine the bird density to be used in the numerical study and found an average density of 950 kg/m^3. The total mass of the bird is 1 kg, which is similar to the mass of an eagle. The eagle is considered because it is one of the largest bird species and can fly at heights of more than 100 m at high speeds. The bird model has a length of 186 mm and a diameter of 93 mm (length-to-diameter ratio of 2:1). The bird model consists of 14,798 nodes and 80,901 tetrahedral elements (C3D4), equivalent to a mesh size of 4.75 mm, which is converted into particles. In this study, the Mie-Grüneisen equation of state (Us-Up) is used to generate pressure profiles during the collision.

The behavior of the bird model during the collision must be validated by comparing the simulated pressure profile with the theoretical calculations, namely the Hugoniot pressure and the stagnation pressure. Validation is carried out by simulating bird strikes on a flat plate. According to Lavoie et al. [18], the collision test was conducted on a plate measuring 305 mm in width and 12.7 mm in thickness, made of Rolled Homogeneous Armor (RHA) steel and clamped around its edges. The collision was conducted perpendicularly with an initial speed of 100 m/s.

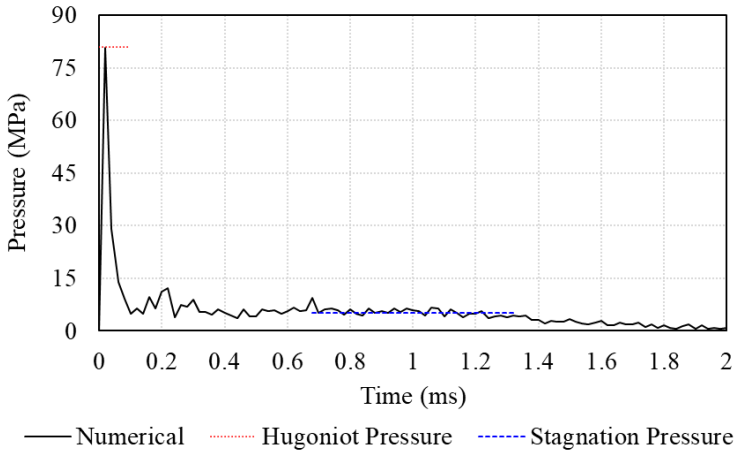

Figure 1 Comparison of numerical simulation pressure and theoretical calculation

The comparison of simulated and theoretical pressures is shown in Figure 1. The Hugoniot pressure (P_H) and stagnation pressure (P_S) show values of 81 MPa and 5.27 MPa, respectively. The stagnation pressure is obtained by calculating the average pressure between 1/3 T and 2/3 T [19]. The numerical value calculated for the stagnation pressure is 5.4 MPa, which corresponds to the theoretical value. A good correlation indicates the effectiveness of the bird model in describing bird behavior. The predicted pressure reflects the theoretical profile, where there is an initial pressure peak followed by a steady-state phase.

In this study, the UAV wing uses the FX 84-W-127 airfoil. The analyzed part of the UAV wing is shown in Figure 2. The wing is modeled with shell elements with a thickness of 0.5 mm and five integration points above and below that thickness. The wing model is fixed at the trailing edge and symmetric boundary conditions are applied in the X-plane as shown in Figure 2(a).

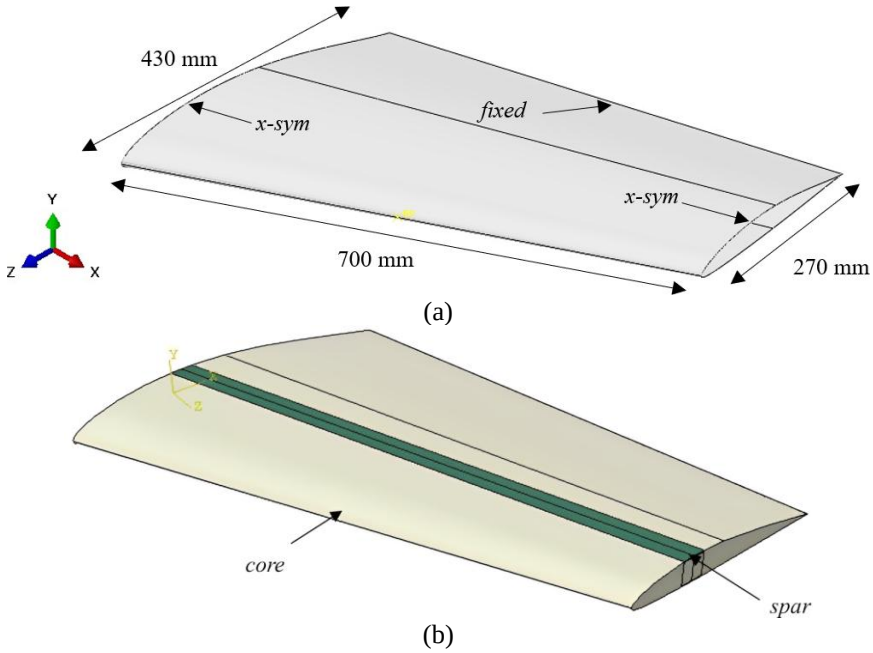

Figure 2 Geometry of the UAV wing and boundary conditions

The construction of the UAV wing consists of skin and internal structure, including the core and spar (see Figure 2(b)). Skin, core, and spar assigned glass fiber reinforced plastic (GFRP), foam (expanded polystyrene foam, EPS), and carbon fiber reinforced plastic (CFRP) materials, respectively. The properties of the GFRP, CFRP, and foam materials adopted from the research of Abdel-Ghany et al. [20] and Shah & Topa [21]. Foam material requires hardening behavior with yield stress and uniaxial plastic strain parameters, obtained from the stress-strain curve [21], and a crushable foam model.

The bird impact test was conducted at various orientation angles, namely 0º, 5º, 10º, and 15º, measured against the bird's longitudinal axis, as shown in Figure 3. These angles were tested to determine the maximum deformation on the leading edge of the UAV wing. Variations in impact angles were conducted because, in reality, the attitude of birds during collisions varies. Therefore, a parametric study on the collision angle between birds and UAV wings is necessary.

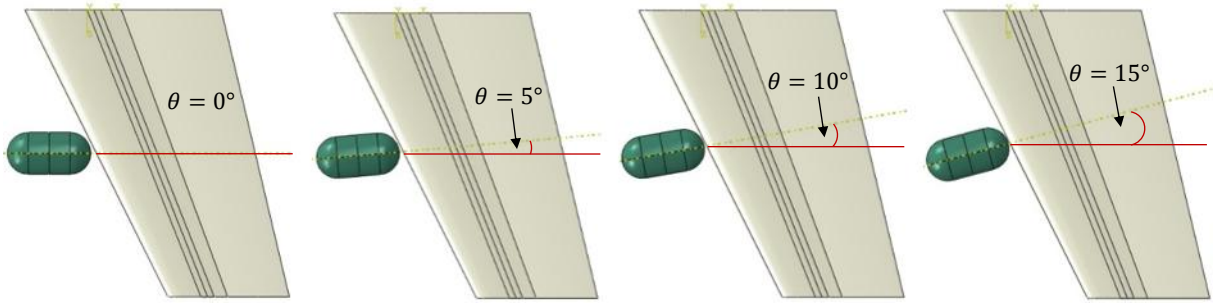

Figure 3 Top view of the scenario showing the variation in collision angles between the bird and the wing

The type of simulation is Dynamic/Explicit with a time of 0.015 seconds, which is considered based on the length of the bird and the collision speed (35 m/s). The collision speed is considered based on the relative speed between the UAV (25 m/s) and the bird (10 m/s) General Contact is used to analyze the contact between the bird and the wing structure as a whole. The interaction between the external and internal structures is defined using Tie Constraints. The element size used is 4 mm based on a mesh convergence study to ensure accurate results.

There are two main aerodynamic forces, namely lift and drag, that act on the airfoil structure as it moves through the airflow. Drag is a parasitic force that acts along the flow direction opposite to the aircraft's motion. The computational fluid dynamics model was implemented to investigate the influence of wing profile changes on airflow, lift, and drag.

If an airfoil is subjected to airflow at a certain angle of attack (α), there is a pressure difference between the upper and lower surfaces. This difference generates a force vector at the aerodynamic center, namely lift and drag. The total lift and drag forces are calculated by integrating the normal and tangential pressure components along the airfoil surface [22]. The integration can be realized through a closed curve that defines the airfoil profile. Equations (1) and (2) are each used to calculate lift and drag forces.

$$L = \oint p\mathbf{n} \cdot \mathbf{k}\mathrm{d}S \tag{1}$$

$$D = \oint p\mathbf{n} \cdot \mathbf{i}\mathrm{d}S \tag{2}$$

Lift and drag forces are denoted by the symbols L and D, while S represents the area of the airfoil, n is the unit vector perpendicular to the airfoil surface, k is the vertical unit vector perpendicular to the airflow direction, and i is the horizontal unit vector parallel to the airflow direction. The values of C_L and C_D are calculated using the lift and drag forces obtained from computational fluid dynamics simulations, using Equations (3) and (4). The air density and air flow velocity are expressed respectively by ρ and v.

$$L = \frac{1}{2}\rho v^2 S C_L \tag{3}$$

$$D = \frac{1}{2}\rho v^2 S C_D \tag{4}$$

The fluid domain is modeled as a C grid to avoid boundary effects. The boundary is located at 15 times the chord line (c) of the airfoil (see Figure 4) [22]. This fluid domain is used in the analysis of aerodynamics performance of undeformed and deformed airfoils. The phenomenon of turbulence behind the wing due to viscosity can be modeled using a fine mesh in the body of influence (boi) section, as shown in Figure 4.

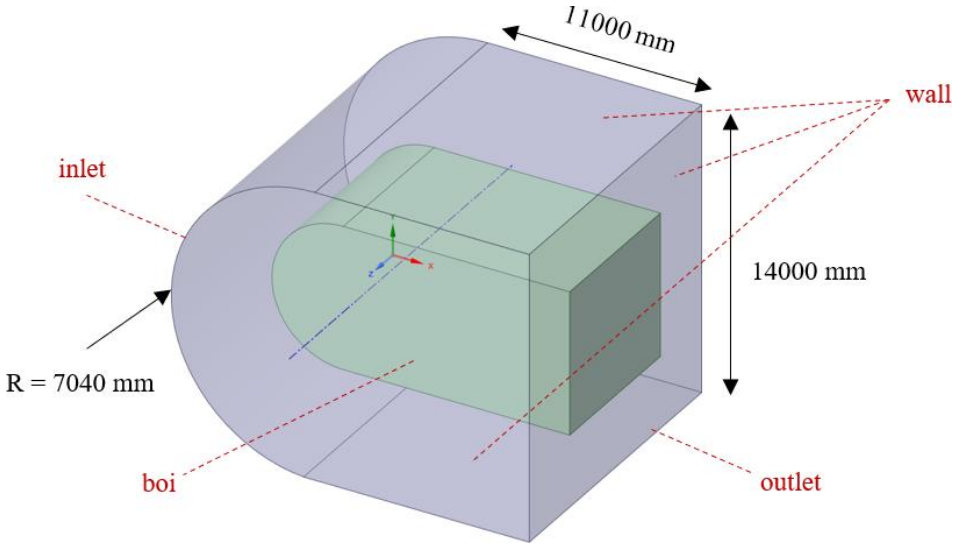

Figure 4 Computational fluid dynamics domain

The air flow velocity is applied at the inlet with sine (sin) and cosine (cos) components to describe the angle of attack (α). The boundary condition of the airfoil surface is enforced as a no-slip wall. The reference pressure needs to be set to provide a relative zero pressure at the outlet. Reference pressure can be determined using Equation (5). The gas constant is denoted by the symbol R, T is the temperature, and ρ is the air density.

$$P = \rho RT \tag{5}$$

$$\rho = \frac{R_e \mu}{uc} \tag{6}$$

The air density varies based on speed and is evaluated using Equation (6). Dynamic viscosity is denoted by the symbol μ, u is the air flow velocity, R is the Reynolds number, and c is the airfoil chord line. The Reynolds-averaged Navier-Stokes (RANS) model is applied with a turbulence model. Poly-hexagonal mesh is applied at locations near or far from the wing. The surface mesh of the wing has a minimum size of 0.002 m and a maximum size of 1 m, while the buoy has a size of 0.2 m.

RESULT AND DISCUSSION

Response of UAV Wing Structure Due to Bird Strike

Figure 5 shows the deformation of the UAV wing due to a bird strike at a 0° angle for various impact times. Deformation increases significantly when the collision duration reaches 6 ms, with the highest-pressure distribution concentrated around the collision area. The maximum deformation indicates the accumulation of kinetic energy from the bird collision. These results are consistent with previous studies [11], [23] which show that deformation due to bird collisions depends on the bird's kinetic energy and the strength of the wing material [24], [25]. However, these results differ from the study by Rezai et al. [26], which showed a more uniform deformation distribution. This is due to the differences in the internal structure of the UAV wing and the properties of the materials used. The UAV wing in this study uses GFRP material in the skin, CFRP in the spar, and foam inside, which combines the rigidity of GFRP and CFRP materials with the flexibility of foam.

Figure 6 shows the deformation of the bird model and UAV wing at a 0° angle with varying collision times. The deformation of the bird model increases with the duration of the collision, indicating the transfer of kinetic energy to the bird's body and the UAV wing. At 15 ms, the bird model was almost completely destroyed, which spread widely across the surface of the UAV wing. These results are consistent with previous research [26] that highlighted the duration of the collision in relation to the level of material damage. However, the bird model shows a more global energy distribution level, unlike the study by Rezaei et al. [26] which focuses more on local deformation. This difference is due to the more detailed bird model in this study.

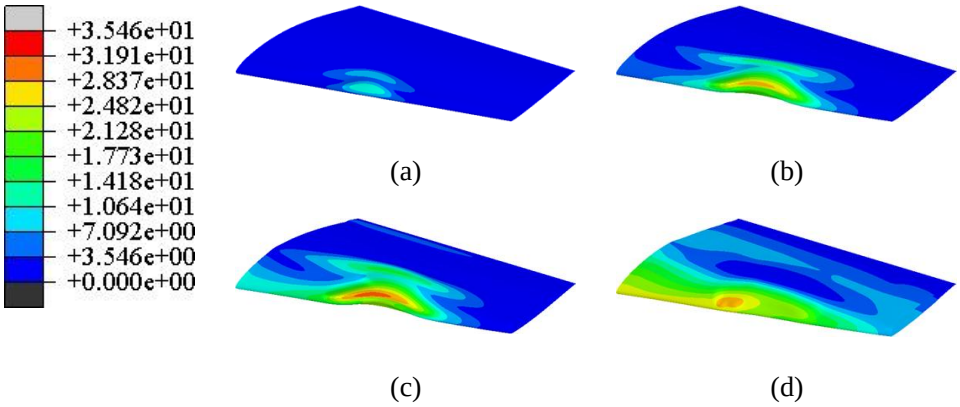

Figure 5 Deformation of the UAV wing after experiencing a bird strike at an angle of 0° and time differences of impact: (a) 1.5; (b) 4.5; (c) 6; and (d) 15 ms

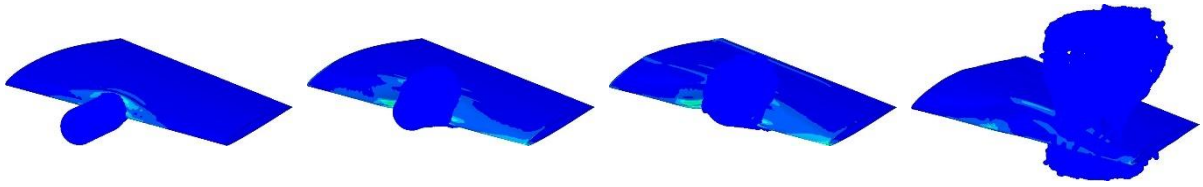

Figure 6 Deformation of the bird model and UAV wing at an angle of 0° and collision time differences: (a) 1.5; (b) 4.5; (c) 6; (d) and 15 ms

Figure 7 shows the displacement of the leading edge of the UAV wing due to bird strikes at different angles. It was found that a collision angle of 0° resulted in a maximum displacement of 22.86 mm, while the displacement decreased at larger angles, indicating the influence of the collision angle on the dynamic response of the structure. This is because the collision energy at a 0° angle is directly absorbed by the wing, while the energy is dispersed at larger angles, there by reducing the displacement. These results are consistent with previous research that showed the angle effect on the distribution of collision energy [16], [27], even though different materials were used. Figure 7 shows that after the bird strikes, leading edge experiences maximum deformation, then oscillates back to a semi-stable state due to the elastic response of the material. The change in impact angle affects the degree of displacement and oscillation because the energy distribution is different.

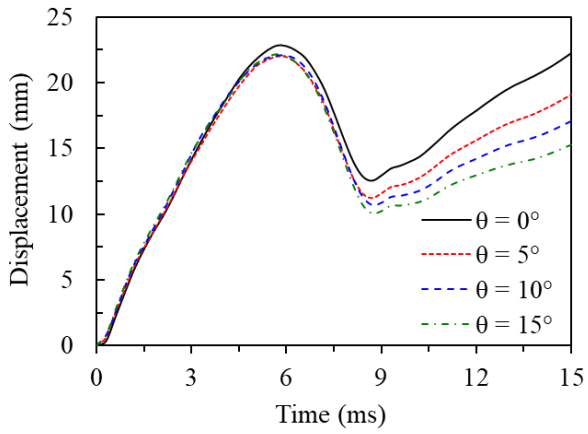

Figure 7 The movement of the UAV wing's leading edge for varying collision angles

Aerodynamic Performance UAV Wing Due to Bird Strike

Fluid dynamics analysis provides pressure distribution around the undeformed airfoil and the deformed airfoil for comparison, as shown in Figures 8 and 9. In Figure 8, the increase from 0° to 30° for the undeformed airfoil results in a greater pressure difference between the upper and lower surfaces.

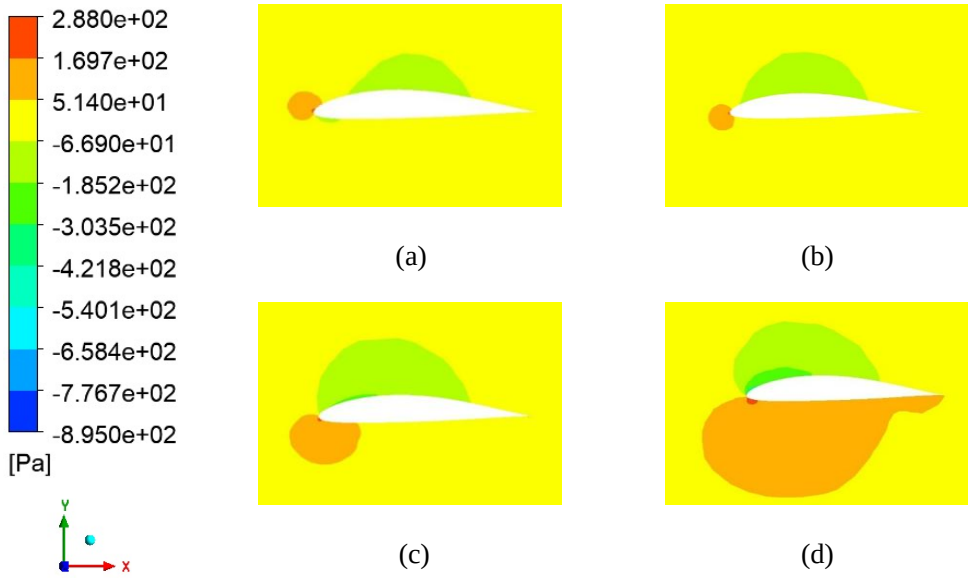

Figure 8 Pressure distribution around the airfoil before deformation at different angles of attack: (a) 0°; (b) 10°; (c) 20°; (d) 30°

Figure 9 shows the pressure distribution for the airfoil that has deformed due to a bird strike. It is evident that the damage to the airfoil disrupts the airflow around it and alters its aerodynamic performance. This is evidenced by the irregular pressure distribution after the wing experienced deformation due to the bird strike. There is only positive pressure on the leading edge and negative pressure on the upper and lower surfaces in most α. The lift force in the collision area drastically decreases due to the negative pressure distribution on most of the airfoil surface.

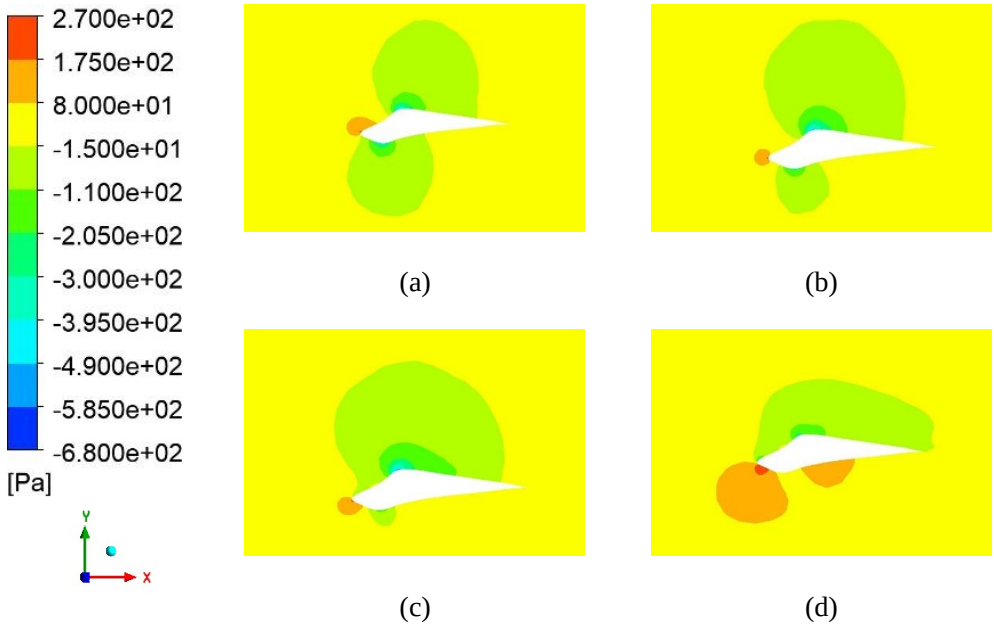

Figure 9 Pressure distribution around the airfoil after deformation at different angles of attack: (a) 0°; (b) 10°; (c) 20°; (d) 30°

The pressure distribution along the airfoil is shown in Figures 10 (a) and (b), for the undeformed and deformed wing profiles. It can be seen that the pressure distribution along the deformed airfoil is disturbed by the damage caused by bird strikes. The pressure difference between the upper and lower surfaces of the airfoil is small, thereby reducing the lift generated.

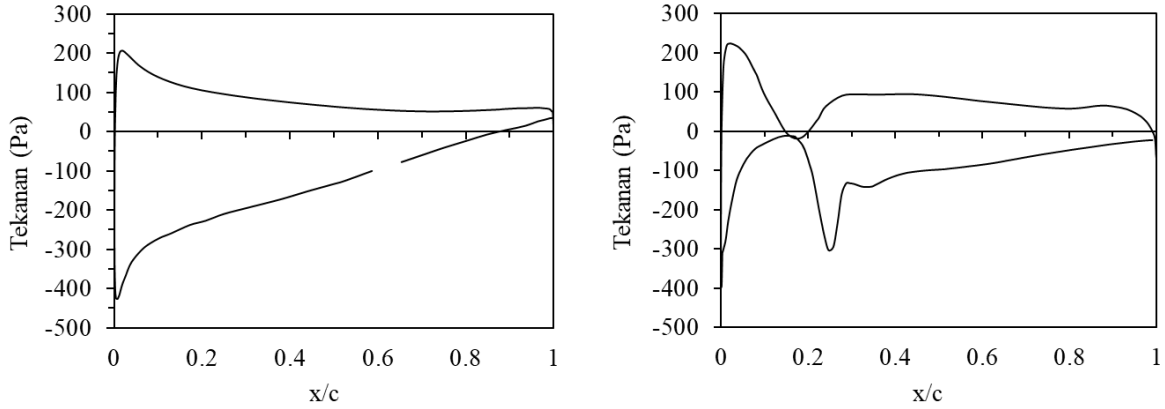

Figure 10 Pressure distribution on (a) an undeformed airfoil and (b) a deformed airfoil at a 30° angle of attack

The lift coefficient (C_L) was obtained from fluid dynamics computations for angles from 0° to 35°, and the results are shown in Figure 11(a). The deformed wing profile shows a lower C_L than the undeformed wing profile at the analyzed α, averaging around 40.8%. Based on the obtained results, C_L has a maximum value of 0.74 for the undeformed wing profile, whereas for the deformed wing, the maximum C_L is 0.55, which occurs α = 30°.

The drag coefficient (C_D) is used to determine the drag force produced by deformed and undeformed wings. Drag not only depends on the complexity of the wing profile and α, but also on the viscosity and compressibility of the air. The compressibility of the air flowing around the UAV wing can be neglected at low speeds. Therefore, in this study, the airflow is considered incompressible, while the air viscosity is assumed to be constant. The changes C_D in the deformed and undeformed wing profiles for angles of attack from 0° to 35° are shown in Figure 11(b). Bird strikes damage the wing profile, causing an increase in the drag coefficient for all tested α values, averaging around 33.4%.

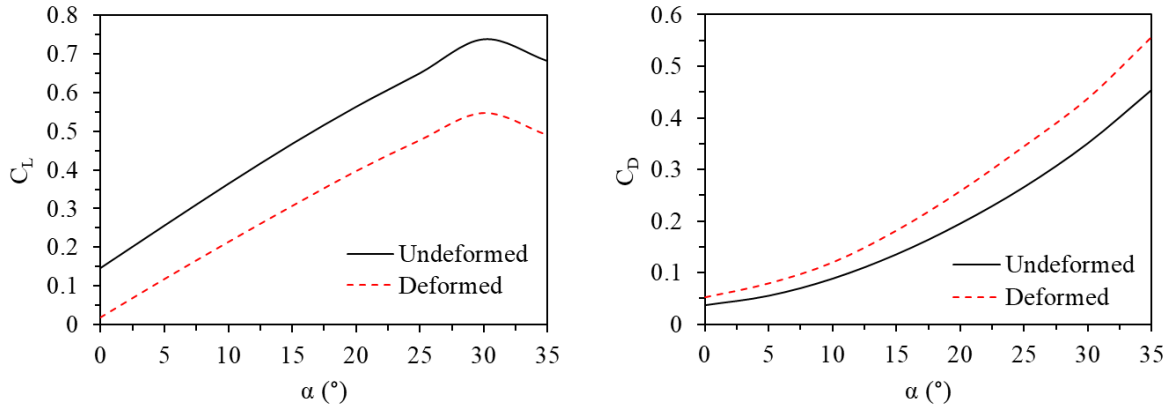

Figure 11 (a) Lift coefficient and (b) drag coefficient for an airfoil experiencing deformation and not experiencing deformation with a difference in α

The lift-to-drag coefficient ratio (C_L/C_D) is a measure of aerodynamic efficiency, which is the amount of lift obtained from the wing compared to the drag caused by the airflow. Figure 12 shows the C_L/C_D ratio from 0° to 35°. It can be seen that the C_L/C_D ratio of the deformed wing decreases significantly compared to the undeformed wing, averaging around 54.8%.

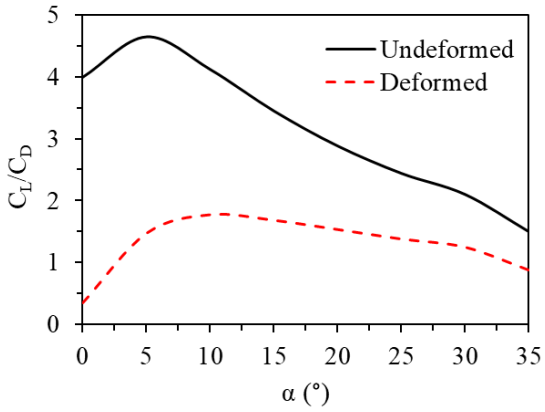

Figure 12 The C_L/C_D ratio of deformed and undeformed airfoil for different α

CONCLUSION

The aerodynamic performance of the UAV wing after a bird strike was analyzed using computational fluid dynamics. In the presented study, the behavior of the bird was modeled using the SPH method for its interaction with the UAV wing. Composite materials including GFRP, CFRP, and EPS foam are applied to the UAV wing structure. The crushable foam model is adopted to address the plastic deformation of the wing structure.

The impact angle significantly affects the distribution of stress and plastic deformation in the wing structure. At the impact angle aligned with the UAV longitudinal axis, the wing experiences higher stress, especially in the area around the leading edge. This indicates that the collision angle results in a greater risk of structural damage. Variations in collision angles also affect the damage patterns, with some angles causing more uniform damage, while others result in concentrated damage in the collision area.

The UAV wing that does not experience deformation has a more stable airflow, uniform pressure distribution, and higher lift coefficient and aerodynamic efficiency, compared to the wing that experiences deformation due to bird strikes at all considered angles of attack. In other words, the deformed wing profile has a reduced lift coefficient compared to the undeformed wing profile at the examined α, averaging approximately 40.8%. The (C_L/C_D) ratio of the deformed wing decreases significantly compared to the undeformed wing, averaging around 54.8%. The deformation of the wing results in an increased drag coefficient by approximately 33.4%, which significantly reduces the aerodynamic performance of the UAV. The disturbed airflow and uneven pressure on the deformed wings cause a decrease in the flight efficiency of the UAV wings.

ACKNOWLEDGEMENT

The author expresses gratitude to Universitas Dirgantara Marsekal Suryadarma for supporting the implementation of this research through the Institute for Research and Community Dedication.

DAFTAR PUSTAKA

[1] B. A. Warsiyanto, S. A. Sitompul, E. Yuniarti, R. Fitriansyah, dan A. B. Utama, "Bird Strike Analysis on 19 Passenger Aircraft Windshield with Different Thickness and Impact Velocity," *Jurnal Teknologi Kedirgantaraan*, vol. 5, no. 2, 2020, doi: 10.35894/jtk.v5i2.5.

[2] S. Y. Chen, W. van de Waerdt, dan S. G. P. Castro, "Design for bird strike crashworthiness using a building block approach applied to the Flying-V aircraft," *Heliyon*, vol. 9, no. 4, 2023, doi: 10.1016/j.heliyon.2023.e14723.

[3] L. Chen, X. Lin, R. Bai, Z. Zhao, dan Z. Guo, "Anti-bird-strike behavior of M40J carbon fiber reinforced plastic laminates," *Compos Struct*, vol. 339, hlm. 118094, 2024, doi: https://doi.org/10.1016/j.compstruct.2024.118094.

[4] G. Lamanna *dkk.*, "Tendency analysis of a tilt rotor wing leading edge under bird strike events," *Forces in Mechanics*, vol. 10, 2023, doi: 10.1016/j.finmec.2023.100173.

[5] B. A. Warsiyanto, S. Fairuza, M. H. Widanto, dan G. Kresna, "Numerical Analysis of Bird Strike on Engine Cowling of AW139 Helicopter using Sandwich Composite Material with Lattice Core Structure," dalam *Proceedings of the 2nd International Conference on Aviation Industry, Education, and Regulation, AVINER 2023, 8-9 November 2023, Jakarta, Indonesia*, EAI, 2024, hlm. 1–17. doi: 10.4108/eai.8-11-2023.2345975.

[6] F. Zhang, G. Luo, H. Zhang, P. Cong, L. Liu, dan W. Chen, "Experimental and numerical analysis study on the low and medium speed bird strike," *Eng Fail Anal*, vol. 156, 2024, doi: 10.1016/j.engfailanal.2023.107766.

[7] Y. Zhang dan Y. Zhou, "Investigation of bird-strike resistance of composite sandwich curved plates with lattice/foam cores," *Thin-Walled Structures*, vol. 182, 2023, doi: 10.1016/j.tws.2022.110203.

[8] H. Kafali dan G. Keskin, "Conceptual design of a gliding UAV for bird strike prevention and observation," *Aircraft Engineering and Aerospace Technology*, vol. 93, no. 1, 2021, doi: 10.1108/AEAT-05-2020-0083.

[9] A. K. Jha, S. Sathyamoorthy, dan V. Prakash, "Bird strike damage and analysis of UAV's airframe," dalam *Procedia Structural Integrity*, 2019. doi: 10.1016/j.prostr.2019.05.051.

[10] S. Wang, X. Zhao, dan J. Huo, "Impact of a bird strike on the aerodynamic performance and damage behavior of a full-scale aeroengine fan," *Aerosp Sci Technol*, vol. 151, hlm. 109270, 2024, doi: https://doi.org/10.1016/j.ast.2024.109270.

[11] M. S. Tatlıer dan T. Baran, "Structural and CFD analysis of an airfoil subjected to bird strike," *European Journal of Mechanics, B/Fluids*, vol. 84, 2020, doi: 10.1016/j.euromechflu.2020.07.012.

[12] L. Xing, Y. Zhang, F. Wang, R. Fu, Z. Sun, dan Y. Li, "Comprehensive effects of aerodynamic performance and dynamic strength of aircraft wings after bird strike in numerical simulation," *Mechanics of Advanced Materials and Structures*, hlm. 1–19, 2024, doi: 10.1080/15376494.2024.2343039.

[13] M. L. Cerquaglia, G. Deliége, R. Boman, dan J. P. Ponthot, "Preliminary Assessment of the Possibilities of the Particle Finite Element Method in the Numerical Simulation of Bird Impact on Aeronautical Structures," dalam *Procedia Engineering*, 2017. doi: 10.1016/j.proeng.2016.12.043.

[14] M. Ugrčić, S. M. Maksimović, D. P. Stamenković, K. S. Maksimović, dan K. Nabil, "Finite element modeling of wing bird strike," *FME Transactions*, vol. 43, no. 1, 2015, doi: 10.5937/fmet1501076U.

[15] R. Hedayati dan M. Sadighi, *Bird Strike: An Experimental, Theoretical and Numerical Investigation*. 2015. doi: 10.1016/C2014-0-02336-2.

[16] A. Riccio, R. Cristiano, S. Saputo, dan A. Sellitto, "Numerical methodologies for simulating bird-strike on composite wings," *Compos Struct*, vol. 202, 2018, doi: 10.1016/j.compstruct.2018.03.018.

[17] J. P. Barber, H. R. Taylor, dan J. S. Wilbeck, "Bird Impact Forces and Pressures on Rigid and Compliant Targets," no. Technical Report AFFDL-TR-77-60. University of Dayton Ohio Research Institute. Air Force Flight Dynamics Laboratory, 1978.

[18] M. Lavoie, A. Gakwaya, M. Nejad Ensan, dan D. G. Zimcik, "Validation of Available Approaches for Numerical Bird Strike Modeling Tools," *International Review of Mechanical Engineering*, vol. 1, no. 4, hlm. 380–389, 2007.

[19] F. Allaeys, G. Luyckx, W. Van Paepegem, dan J. Degrieck, "Numerical and experimental investigation of the shock and steady state pressures in the bird material during bird strike," *Int J Impact Eng*, vol. 107, 2017, doi: 10.1016/j.ijimpeng.2017.05.006.

[20] A. W. Abdel-Ghany, I. Taha, dan S. J. Ebeid, "Failure Prediction of Fiber Reinforced Polymer Pipes using FEA," 2016.

[21] Q. H. Shah dan A. Topa, "Modeling large deformation and failure of expanded polystyrene crushable foam using LS-DYNA," *Modelling and Simulation in Engineering*, vol. 2014, 2014, doi: 10.1155/2014/292647.

[22] J. D. Anderson, *Fundamentals of Aerodynamics (6th edition)*, vol. 1984, no. 3. 2011.

[23] B. A. Warsiyanto, A. Nurrohmad, R. Fitriansyah, A. B. Utama, S. A. Sitompul, dan E. Yuniarti, "An Investigation of Dynamic Response of 19 Passenger Commuter Aircraft Windshield against Bird Strike," 2021.

[24] J. Ćwiklak, E. Kobiałka, dan A. Goś, "Experimental and Numerical Investigations of Bird Models for Bird Strike Analysis," *Energies (Basel)*, vol. 15, no. 10, 2022, doi: 10.3390/en15103699.

[25] I. Talhah dan P. Hampson, "Smooth particle hydrodynamics birdstrike analysis on aircraft wing leading edge," *International Journal of Multiphysics*, vol. 15, no. 3, 2021, doi: 10.21152/1750-9548.15.3.291.

[26] M. Rezaei, B. Arezoo, dan S. Ziaei-Rad, "Redesign an aircraft windshield to improve its mechanical resistance against simultaneous bird impacts," *Int J Impact Eng*, vol. 184, 2024, doi: 10.1016/j.ijimpeng.2023.104811.

[27] J. F. Ramírez *dkk.*, "Numerical Modeling and Simulation of Uniaxial Compression of Aluminum Foams Using FEM and 3D-CT Images," *Procedia Materials Science*, vol. 4, 2014, doi: 10.1016/j.mspro.2014.07.609.